

## Material Properties

# Fabrication of exfoliated graphite reinforced silicone rubber composites - Mechanical, tribological and dielectric properties

P.S. Sarath<sup>a</sup>, Sohil Varghese Samson<sup>a,b</sup>, Rakesh Reghunath<sup>c</sup>, Mrituanjay Kumar Pandey<sup>d</sup>, Józef T. Haponiuk<sup>e</sup>, Sabu Thomas<sup>f</sup>, Soney C. George<sup>a,\*</sup>

<sup>a</sup> Centre for Nanoscience and Technology, AmalJyothi College of Engineering, Kanjirappally, Kottayam, Kerala, India

<sup>b</sup> Department of Mechanical Engineering, AmalJyothi College of Engineering, Kanjirappally, Kottayam, Kerala, India

<sup>c</sup> Department of Mechanical Engineering, NSS College of Engineering, Palakkad, Kerala, India

<sup>d</sup> Directorate of Extramural Research and Intellectual Property Right, Defence Research and Development Organisation (DRDO), New Delhi, India

<sup>e</sup> Department of Polymer Technology, Gdansk University of Technology, Gdańsk, Poland

<sup>f</sup> International and Inter University Centre for Nanoscience and Nanotechnology, Mahatma Gandhi University, Kottayam, Kerala, India



## ARTICLE INFO

## Keywords:

Silicone rubber  
Exfoliated graphite  
Tribology  
Dielectric performance

## ABSTRACT

The effect of exfoliated graphite (EG) on the mechanical, tribological and dielectric properties of the silicone rubber (QM) composites has been systematically investigated and analysed. Morphological analysis of the composites helps to understand the interfacial interaction between the filler and the rubber matrix as well as wear mechanism respectively. An enhancement in the mechanical, tribological and dielectric properties was observed with an increase in filler loading and better performance was observed at 7 phr of filler loading. The improvement in performance is attributed to the better interaction between the QM chains and the EG layers as evident from the AFM and TEM analysis. It is also evident from the Kraus plot which supports the reinforcing effect of EG in QM matrix.

## 1. Introduction

Tailoring of elastomeric composites by the addition of fillers has gained wide popularity over the years. The fact that properties of elastomeric composites could be improved has led many researchers to develop high performance composites using different elastomers and filler combinations [1–4]. Among the many types of fillers, graphite-based filler was used for this research work based on a detailed investigation by Sadasivuni et al. [5]. Silicone rubber has numerous applications in fields such as mechanical, electrical, thermal and insulation [6], but the area such as tribological aspects are yet to be explored. Research conducted by Lee and Ji [7] reveals that silica reinforced silicone rubber has resulted in improved dielectric strength. Further, varying the vinyl content in the rubber matrix has led to improved hardness and tracking resistance. Using dopamine coated barium titanate as fillers in silicone rubber, a new soft dielectric elastomer composite was successfully prepared by Jiang et al. [8]. It is observed that fillers were highly compatible in the rubber matrix and helped to improve the electro-mechanical properties. Du et al. [9] were

successful in blending polydimethylsiloxane modified gelatin/silicone rubber to fabricate an asymmetric bilayer membrane having porous structure. These findings suggest an excellent bio-medical application of silicone rubber. The researchers promise that this membrane act as a substitute platform for skin regeneration because the mechanical properties, water uptake and water vapor permeability meets usual wound dressing material requirements. Surface treated halloysite nanotube (HNT) was incorporated into silicone rubber to study the effects of HNT loading on its mechanical and thermal properties [10]. Increased stiffness, tensile strength and improved thermal stability were witnessed in the developed nanocomposite with increasing filler loading. Xu et al. [11] reported a feasible method in blending poly (vinylidene fluoride) and methyl vinyl silicone rubber to develop a thermoplastic vulcanizate. This vulcanizate showed excellent mechanical properties. Silicone rubber foam with enhanced mechanical performance was developed by using nanographite as filler [12]. Microcellular changes in the composites such as improved cell density and reduced mean cell diameter was obtained. These changes increased the compressive strength and enhanced the thermal stability of the silicone rubber/nanographite

\* Corresponding author. Centre for Nanoscience and Technology, AmalJyothi College of Engineering, Kanjirappally, Kottayam, Kerala, India.

E-mail addresses: [sarathps005@gmail.com](mailto:sarathps005@gmail.com) (P.S. Sarath), [sohiledu@gmail.com](mailto:sohiledu@gmail.com) (S.V. Samson), [rakeshreghunath@amaljyothi.ac.in](mailto:rakeshreghunath@amaljyothi.ac.in) (R. Reghunath), [mkpandey@hqr.drdo.in](mailto:mkpandey@hqr.drdo.in) (M.K. Pandey), [jozef.haponiuk@pg.gda.pl](mailto:jozef.haponiuk@pg.gda.pl) (J.T. Haponiuk), [sabuthomas@mgu.ac.in](mailto:sabuthomas@mgu.ac.in) (S. Thomas), [sonygeo@gmail.com](mailto:sonygeo@gmail.com) (S.C. George).

<https://doi.org/10.1016/j.polymeresting.2020.106601>

Received 10 February 2020; Received in revised form 19 April 2020; Accepted 4 May 2020

Available online 14 May 2020

0142-9418/© 2020 Elsevier Ltd. This is an open access article under the CC BY-NC-ND license (<http://creativecommons.org/licenses/by-nc-nd/4.0/>).

foam.

Graphene, a wonder material of this era, has also been used as fillers in silicone rubber. The addition of graphene nanoplatelets in silicone rubber has enhanced the tensile strength, thermal conductivity and thermal stability [13]. Even graphene nanoribbon incorporation in silicone rubber has lead to the increase of thermal and mechanical properties of the nanocomposites [14]. One of the latest methods of manufacturing technique is 3D printing. Quite surprisingly, carbon fiber reinforced silicone rubber composites were successfully 3D printed by Huang et al. [15]. These conductive composites were developed for strain sensor applications. Also, they were found to have excellent mechanical properties. Pylios et al. [16] used medical grade silicone rubber which is tested on pin-on-disc apparatus against titanium and Ultrahigh Molecular Weight Polyethylene (UHMWPE) to study the wear properties. Titanium pin produced less wear on the rubber composites when compared to UHMWPE under dry sliding conditions and under the effect of lubricants. The effects on the mechanical and tribological properties of different white carbon black were investigated by He et al. [17]. The prepared composites showed excellent mechanical and anti-wear properties.

However, very few works have been reported with QM reinforced graphite-based fillers when compared to other types of elastomers especially in the field of tribology. Therefore, silicone rubber with exfoliated graphite as reinforcing filler is selected for this research work. Later the studies were extended to tribological properties such as coefficient of friction, wear rate of the composites in detail and it is correlated with the morphological analysis of the worn surface.

## 2. Experimental details

### 2.1. Materials

The elastomer matrix used for this research work was silicone rubber (QM) 5060-U grade procured from KPCC Corporation, Korea. The reinforcing filler, exfoliated graphite (EG) was collected from Asbury Carbons, USA. Dicumyl peroxide (DCP), the curing agent was procured from Sigma Aldrich, Bangalore, India. Other ingredients and solvents used were of laboratory grade and were used without further purification.

### 2.2. Preparation of composites

Two-roll mixing technique was used for the preparation of composites. The rubber matrix, filler and the curing agent were thoroughly mixed according to the formulations given in Table 1. The mixing of each sample consumed about 20 min. Optimum cure time of the rubber vulcanizates was determined according to ASTM D-1646 in an oscillating disc type rheometer. The samples were press-cured for their respective cure time at 150 °C and post cured at 200 °C for 4 h in a hot oven. The preparation layout of silicone rubber/exfoliated graphite composite (QMEG) is shown in Fig. 1.

### 2.3. Characterization and tests

#### 2.3.1. Structural characterization

The structural characterization of composites was carried out by X-ray diffraction (XRD) analysis in Bruker AXS D8 advance X-ray

**Table 1**  
Compounding ingredients of silicone rubber exfoliated graphite composites (Phr)<sup>a</sup>.

Ingredients (phr)	QM	QMEG3	QMEG5	QMEG7	QMEG10	QMEG12	QMEG15
QM	100	100	100	100	100	100	100
EG	0	3	5	7	10	12	15
DCP	1.5	1.5	1.5	1.5	1.5	1.5	1.5

<sup>a</sup> Parts per hundred parts of rubber.

diffractometer. X-ray source - Cu K $\alpha$  radiation ( $\lambda = 0.154$  nm).

#### 2.3.2. Diffusion studies

The data obtained from solvent diffusion studies was used for investigating the reinforcing effect of the composites. Diffusion studies were performed as per the following procedure (at room temperature conditions). Circular samples were punched out from the compression moulded sheet using sharp edged steel die. The thickness of the samples was measured using micrometer screw gauge. Initial weight of the samples was noted in a precise electronic balance. Further, it was soaked in 25 ml toluene (solvent) in sorption bottles. At regular intervals, samples were taken out, its surface wiped off gently to remove the adhere solvent, weighed and placed back in the test bottles consuming around 30 s. The weighing was repeated till equilibrium was attained and the diffusion parameters were calculated.

#### 2.3.3. Mechanical tests

The mechanical properties of the elastomeric composites were tested in a pneumatic universal testing machine, INSTRON-4411 with a grip separation of 30mm and cross head velocity of about 500 mm/min. Dumbbell specimens were punched out of the moulded sheet and thickness of the narrow portion was measured. Each specimen was placed tightly between the two grips whose upper grip being fixed and experiment was conducted. The tensile strength, elongation at break, modulus (tensile test as per ASTM D412) and tear strength (tear testing as per ASTM D624) values were recorded. The hardness measurements were carried out using a shore Adurometer (DPX-1000, Rex Gauge Co., USA) following the ASTM D2240 standard.

#### 2.3.4. Tribological tests

To understand the tribological features of the developed composites, two types of wear tests were carried out on the filler reinforced elastomeric specimens in order to study their friction and wear properties – two body and three body wear tests. 2.3.4.1. Two body wear tests.

Two body wear studies were conducted on pin-on-disc machine as per ASTM G99 standards as shown in Fig. 2. After noting the initial weight of the pin shaped specimens, they are subjected to an initial run-in period so that the specimen surface comes in complete contact with the disc surface. The pin gets rubbed against a rotating steel disc (EN -32) of hardness HRC 65 with a track diameter of 100 mm under loaded condition. Coefficient of friction between the pin and the disc is measured by the deflection occurring in the calibrated load cell. The experiment is conducted for different loads, sliding distances, and temperatures and the detailed experimental operating condition are listed in Table 2.

After completion of the tests, the specimen pins are cleaned with acetone and dried. Their final weights are noted for determining the weight loss from which the wear rates are calculated. The equipment monitor displays the generated tangential frictional force when the specimen starts to

rub the counter face and this force is recorded to calculate the coefficient of friction ( $\mu$ ) as follows:

$$\mu = F_f / F_n \quad (1)$$

Where  $F_f$  (frictional force) and  $F_n$  (normal load which is applied). The specific wear rate ( $W_s$ ) is calculated by:

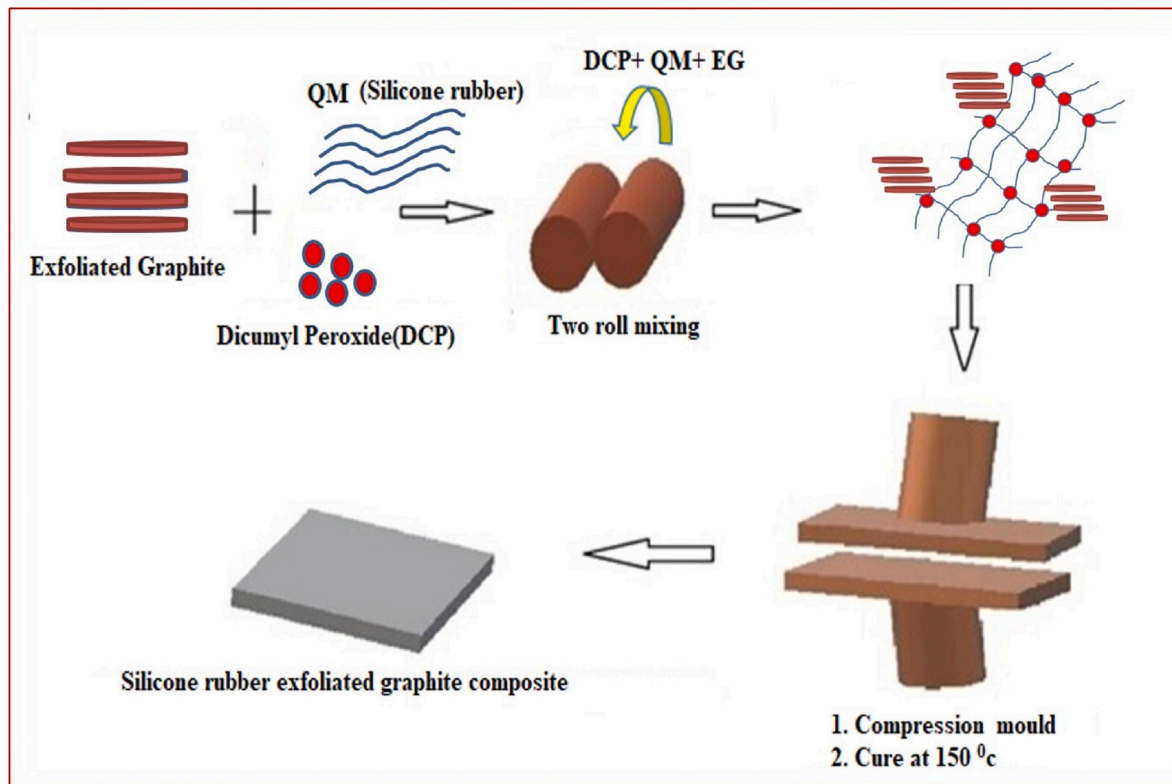


Fig. 1. Schematic representation of preparation of the QMEG composite.

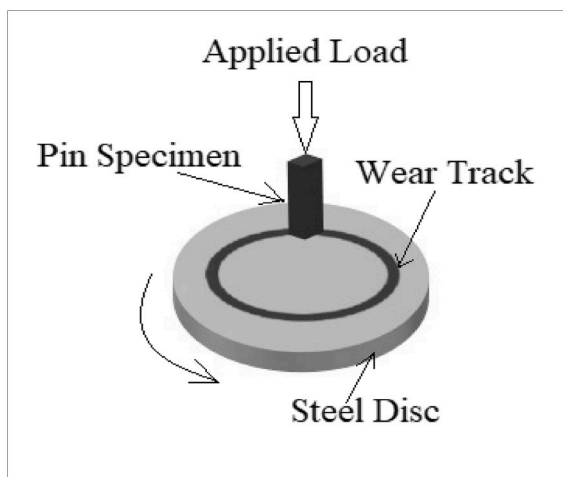


Fig. 2. Schematic representation of pin-on-disc test.

Table 2  
Detailed experimental operating conditions.

Parameters	Operating Conditions
Temperature	Ambient conditions (temperature: 29 °C)
Relative humidity	55(±5) %
Test disc	Hardened ground steel (EN 31, hardness 60 HRC)
Roughness of EN-31	1.6 m Ra
Rubbing duration	1800s
Load	10 N, 20 N and 30 N
Sliding speed	1 m/s, 2 m/s, 3 m/s and 5 m/s
Sliding distance	1800 mm and 3600 mm
Pin size (ASTM G99 Std.)	30 mm × 10 mm × 10 mm

$$W_s = \Delta m / \rho F_n L \tag{2}$$

Here  $\Delta m$  is the weight loss,  $\rho$  is the composites' density,  $F_n$  is the applied load and  $L$  is the sliding distance (meters).

2.3.4.1. *Three body wear tests.* A dry rubber wheel abrasive wear test rig is used to conduct three body wear studies according to ASTM G65 as shown in Fig. 3. The test specimen of size 76 mm × 25 mm × 2 mm, gets abraded by using dry sand as the abrasive particle which is introduced in between the test specimen and the rotating wheel (rotated at a speed of 2 m/s) with a chorobutyl rubber tire in a controlled flow rate. The wheel rotates in such a way that its contact face moves in the direction of sand flow. The wear tests are carried out for different load conditions. Abrasive particles used are silica sand (AFS 50/70) of size 150–300 μm and the sand flow rate between rubber wheel and specimen is 375 ± 5 g/

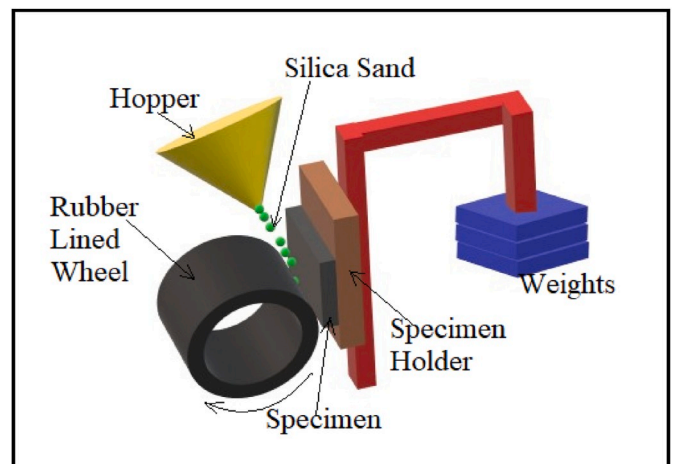


Fig. 3. Schematic diagram of dry sand/rubber wheel abrasive wear test rig.

min. The wear rate, determined from the measured weight loss values of the specimens, is further converted to wear volume. The specific wear rate ( $K_s$ ) is calculated by the equation;

$$K_s = \frac{V}{F_n \times L} \quad (3)$$

Where, V- Volume loss (wear)

$F_n$ - Applied Load

L - Sliding distance (meter)

### 2.3.5. Dielectric tests

Dielectric studies of the composites were performed in Agilent E4980A precision LCR meter (frequency range: 100 Hz to 2 MHz). AC conductivity, dielectric loss and dielectric permittivity (as per ASTM D150) values were obtained from these tests.

### 2.3.6. SEM(Scanning electron Microscopy)Analysis

The tensile fractured surface and the worn surface morphology of composites were analysed using TESCAN VEGA 3 SBH; (Thermal Emission) with resolution of 3 nm/30 KV. The samples to be analysed were sputter coated using Quorum SC7620 with Gold-Palladium.

## 3. Results and discussion

### 3.1. Structural characteristics - XRD analysis

Fig. 4 illustrates the X-ray diffraction patterns of neat QM, EG along with QMEG7 composite. EG exhibits a high crystalline degree with a strong, sharp diffraction peak at  $2\theta = 26.38^\circ$  with d-spacing of 3.37 Å. The sharp reflection at  $2\theta = 26.4^\circ$  is once again observed in QMEG7, which implies that the individual EG sheets consist of multilayer graphite sheets with a d-spacing of 3.4 Å. Intrusion of polymer molecules does not change the structure of graphite, and hence its crystal structure is retained. Silicone rubber shows a broad peak at  $11.28^\circ$  with d-spacing value 7.84 Å. For the composite, as light change in peak position and d-spacing are observed.

The introduction of a filler into an elastomeric matrix leads to the formation of a reinforced composite materials. The extent of

reinforcement depends on several factors such as filler loading, filler-filler interaction, polymer-filler interaction, hydrodynamic effect, degree of cross linking etc. [18]. Thus the vulcanization characteristics are also depends on these factors normally. The vulcanization characteristics of the composites could be studied by analyzing the cure characteristics given in Table 3. The minimum torque ( $M_L$ ) values in the table present as the minimum viscosity and it represent the measure of mastication [19].  $M_L$  values increased with increase in EG content and it indicate the building up of viscosity. The increase in viscosity with EG content reveals that filler restrict the movement of silicone chains and the processability becomes harder. It is clear from Table 3 that the maximum torque ( $M_H$ ) values increased with increase in the concentration of EG and thereby the stiffness of the vulcanizate is improved. The details of the extent of crosslinking reactions, and the shear modulus of the vulcanizate can be infer from the  $M_H$  values. Moreover it also provide an idea about the filler-polymer interactions. Therefore it is easy to understand from  $M_H$  values that the extent of crosslinking, shear modulus as well as filler-polymer interactions are improved at higher dosage of EG. The differential torque,  $\Delta S$  (i.e.  $M_H - M_L$ ) represent the extent of crosslinking between silicone rubber and the curing agent. These results indicate that,  $\Delta S$  for filled samples are higher than that of pure rubber. Thus  $\Delta S$  increased with EG content. Scorch time ( $t_{s2}$ ) is a parameter which measure the premature vulcanization of the composite and it evident from Table 3 that scorch safety increased with increase in the concentration EG. In order to get optimum physical properties the samples are usually vulcanized at optimum cure time ( $t_{90}$ ). As in the case of  $M_H$  and  $M_L$ , the  $t_{90}$ , also increased with increase in EG Content. The cure rate index (CRI) is a parameter which represent the fastness of curing process. The CRI values given in Table 2 showed that the highest values was observed for pure silicone rubber sample and the lowest for silicone rubber with higher filler content. Thus CRI values decreased with increase in EG content. This may be due to the improved surface area of EG that prevents the accelerating effect in vulcanization process [20].

### 3.2. Mechanical properties

Silicone rubber has weak intermolecular forces among polymer chains. Thus, it has lower mechanical strength and this paves a way to improve its mechanical properties by incorporating fillers within its matrix. The various mechanical properties obtained for different EG filler loadings are shown in Table 4.

QMEG7 shows dispersion of EG with maximum tensile strength of 6.8 MPa which is almost 30% higher than QM. From the table, it is clear that tensile strength increases with filler loading up to 7phr and it decreases further. This reduction in value occurred because of agglomeration of EG particles. Agglomeration has affected dispersion and interaction of fillers within the rubber matrix. The effective dispersion of EG in matrix has facilitated uniform transfer of stress throughout rubber matrix. QMEG7 shows the optimum tensile strength, elongation at break and tear strength properties. This is because EG layers have been able to uniformly disperse in the elastomer matrix. Hardness values are also found to be increased continuously with EG filler concentrations as

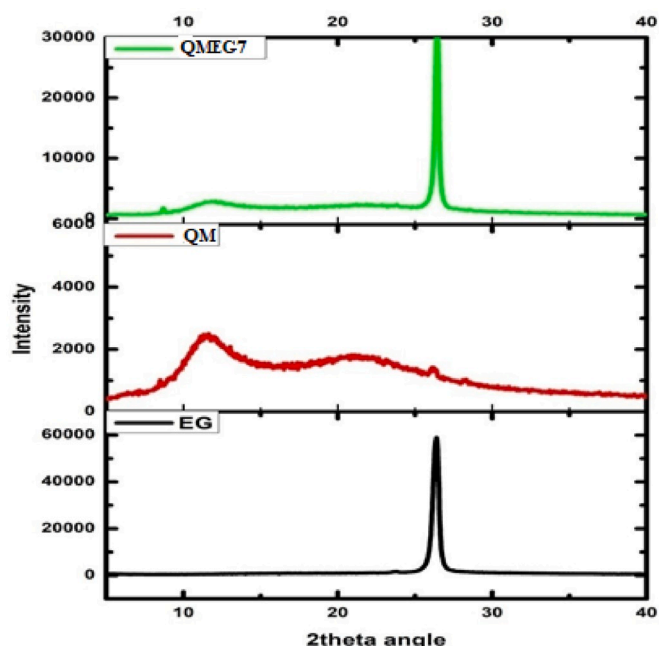


Fig. 4. X-ray powder diffraction patterns.

Table 3  
Cure characteristics of composites.

Sample	$M_L$ (dNm)	$M_H$ (dNm)	$\Delta S$ (dNm)	Scorch Time( $t_{s2}$ ) (min)	$t_{90}$ (min)	Cure rate index(CRI) $\text{min}^{-1}$
QM	0.65	12.90	12.25	0.86	5.76	20.40
QMEG3	0.71	13.37	12.66	0.93	6.56	17.76
QMEG5	0.72	13.74	13.02	1.00	7.54	15.29
QMEG7	0.78	13.97	13.19	0.96	7.13	16.20
QMEG10	0.77	14.73	13.96	1.02	7.74	14.88
QMEG12	0.81	14.75	13.94	1.06	8.93	12.70
QMEG15	0.83	14.84	14.01	1.06	9.42	11.96

**Table 4**  
Mechanical properties of composites.

Sample	Tensile strength (MPa)	Elongation at break (%)	Modulus at 100% (MPa)	Tear strength (N/mm)	Hardness (Shore A)
QM	4.747 ± 0.33	198 ± 12	2.36 ± 0.20	20.45 ± 1.24	51 ± 4
QMEG3	5.98 ± 0.12	241 ± 20	2.96 ± 0.25	24.81 ± 2.20	57 ± 4
QMEG5	6.589 ± 0.23	226 ± 16	3.53 ± 0.40	27.84 ± 3.10	63 ± 4
QMEG7	6.811 ± 0.21	221 ± 12	3.86 ± 0.30	30.22 ± 2.40	65 ± 2
QMEG10	6.184 ± 0.12	190 ± 18	4.21 ± 0.40	30.19 ± 2.34	67 ± 4
QMEG12	5.544 ± 0.32	150 ± 8	4.45 ± 0.40	29.82 ± 2.10	67 ± 2
QMEG15	5.446 ± 0.22	143 ± 10	4.87 ± 0.50	26.15 ± 3.20	69 ± 4

stiffening of elastomeric chains occurred with filler loading.

### 3.2.1. Tensile fracture surface morphology

A better knowledge of the interfacial adhesion between filler and rubber matrix can be obtained through the observation of tensile fractured surface as shown in Fig. 5. Fig. 5(a) shows the SEM image of neat EG with graphitic layers and Fig. 5(b) reveals silicone rubber with a very smooth surface. In the case of QMEG5 composites fracture surface appears to be much rougher and some voids noticed from the composites. But partially intercalated layers of the QMEG5 are visible in the SEM image. This is responsible for the enhancement of mechanical properties exhibited by QMEG5. Meanwhile, QMEG7 composites shows a better smooth surface with relatively low number of voids. It support its superior mechanical properties. Increased filler loading (QMEG10 composite), decreases the surface smoothness of the composites. This indicates that beyond 7 phr filler loading, agglomeration starts, it affect

the dispersion and interaction between filler and matrix.

SEM images suggests that polymers are able to enter into the graphitic layers and forms interfacial interactions which has improved the mechanical properties of the composites. The dispersed EG, acts as a large number of stress concentration points in the QM matrix which absorbs energy and helps to transfer the load uniformly throughout the matrix as in the case of QMEG7 composite. Further it hinders crack growth under a strong external shock. Further QMEG composites reinforcement mechanism can be explained using Kraus plot (Fig. 6).

Based on Kraus equation as shown below [26],

$$\frac{V_{r0}}{V_{rf}} = 1 - m \left( \frac{f}{1-f} \right) \quad (4)$$

Where,  $V_{r0}$ -volume fraction of the swollen polymer in the fully swollen unfilled sample.

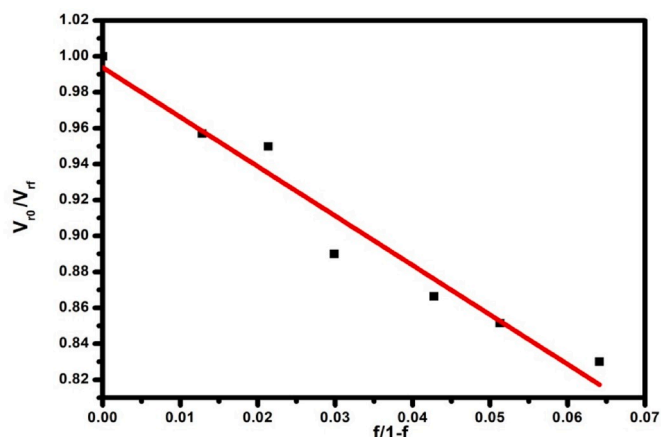


Fig. 6. Kraus plot of QMEG composites.

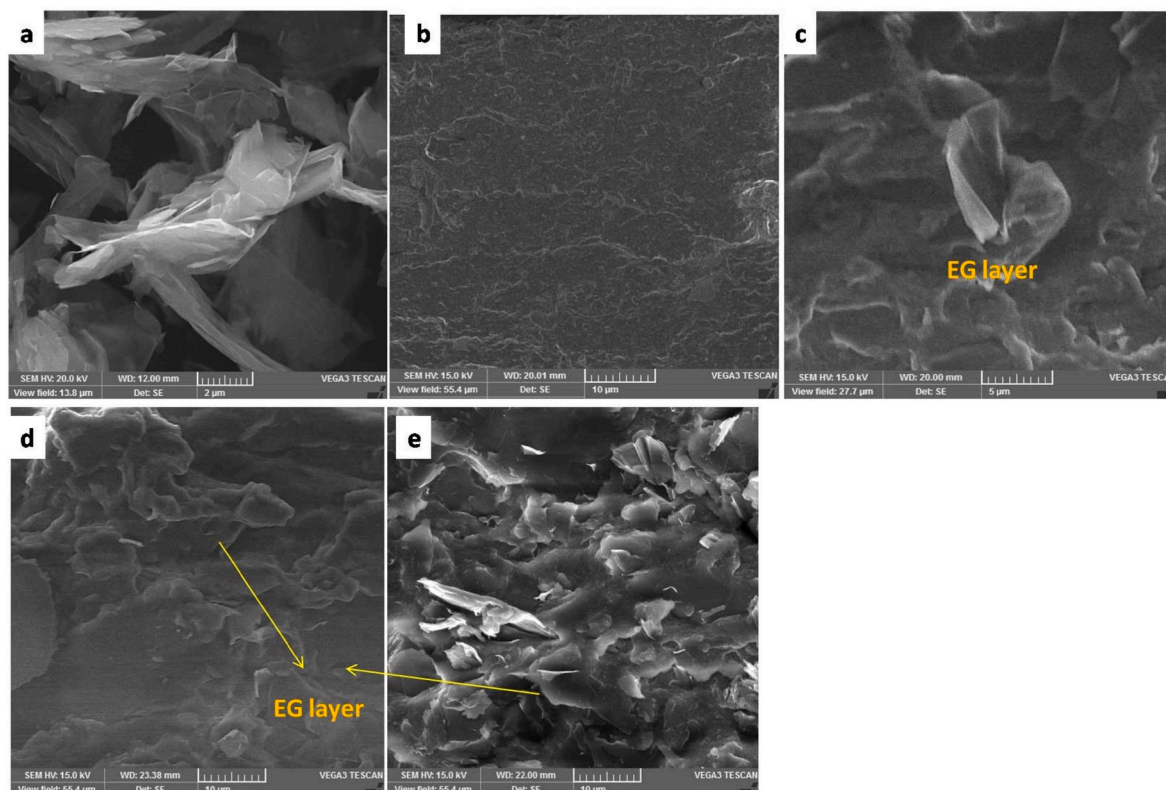


Fig. 5. Fracture surface SEM images (a) EG pure (b) QM (c) QMEG5 (d) QMEG7 and (e) QMEG10.

$V_{rf}$ -volume fraction of the swollen reference polymer in the fully swollen filled sample

$f$  - volume fraction of the filler

$m$  - slope is a direct measure of the reinforcing capacity of the filler in the matrix.

Fig. 6 gives the plot of  $\frac{V_{r0}}{V_{rf}}$  vs  $\left(\frac{f}{1-f}\right)$ . As the filler loading increases the value of  $\frac{V_{r0}}{V_{rf}}$  decreases. Therefore, the composite with highest filler loading has the least value.

According to Kraus theory, higher the negative value of the slope, greater the reinforcement of the matrix with the filler. ( $V_{r0}/V_{rf}$ ) is less than unity and the value of this ratio decreases with filler loading in QMEG composites. In QMEG composites ( $V_{r0}/V_{rf}$ ) is 0.95 for 3 phr EG and 0.83 for 15 phr EG, indicate better reinforcement of EG with matrix [21]. As the reinforcement increases, the degree of transfer of stress from polymer matrix to filler will increase, which leads to an increase in the constraint zone of polymer chains.

### 3.3. Tribological properties

#### 3.3.1. Friction and wear properties [Two body wear tests]

Fig. 7 provides information regarding the COF as a function of time (s) and the specific wear rate ( $\text{mm}^3/\text{Nm}$ ) of the composites for different amount of filler loading.

Fig. 7(a) depicts the variation of coefficient of friction with respect to the sliding time. It is found that frictional coefficient values for all the composites shoot up initially and then a gradual decrease is observed to finally achieve almost stable values. It is also noticed that coefficient of friction of the EG filled composites is much lower than that of pure silicone rubber. Composite with 7 phr filler loading exhibited lowest COF value. However, QMEG10 composite quickly stabilized its COF value. Fig. 7(b) shows the variation of specific wear rate of composites with respect to graphite content. The specific wear rate of EG loaded composites is also found to achieve a lower value when compared to that of neat sample with lowest value for 7 phr loaded sample.

Thus, it is clear that EG reinforcement enhances the tribological properties of the composites. The self-lubricating property of graphite has in fact played a major role in achieving a lower COF and specific wear rate value. EG forms a transfer film on the frictional surface of the counterpart during rubbing which acts a lubricating film to help decrease these values. As the time increases, more and more stable film formation occurs [22]. A reduction in COF will also help to reduce the wear rate. Addition of filler concentration up to 7phr decreases the friction coefficient and specific wear rate after which friction coefficient and specific wear rate starts to increase indicates that the optimum limit

– 7 phr has been reached.

**3.3.1.1. Influence of normal load.** The effect of applied load on COF and specific wear rate of the composites is analysed with the data shown in Fig. 8 (a) and (b.) As the load is increased, COF and wear rate of EG filled composites have a low value when compared to pure QM sample. At low loads (10 N) the COF and wear rate are quite high. Lower loads are unable to chip off the EG layers from the surface as such the applied load of 10 N is insufficient to break the interfacial adhesion existing between the EG filler and the matrix rubber. This leads to increased friction between the surface and in turn leads to higher wear rates. As the load reaches 30 N there is a drastic reduction in COF and increase in specific wear rate.

**3.3.1.2. Influence of sliding velocity.** Fig. 8 (c) and (d) represents the effect of filler reinforcement of composites on the COF and specific wear rates by varying the sliding velocity. As the EG content increases friction and wear properties decreases. Samples subjected to low sliding velocity (1 m/s) is characterised by higher friction and wear properties when compared to the sample values at higher sliding velocity (5 m/s). The values of COF and wear rates of composites with EG fillers are much lower to that of neat QM sample. Here also it is observed that 7 phr is the optimum value. When the specimen is rotated at 1 m/s, effective contact between the rubber and counter face takes place. Therefore, pure sample is observed to have high COF and wear rate values. However, with the addition of filler, EG gets peeled off from the rubber matrix for the applied load to form lubricant films thus reducing the contact area between the rubber and the counterpart leading to a reduction in these values. Meanwhile, at 5 m/s much films are not generated and even if any films are generated, this velocity might have affected the films stability to remain between the rubbing surfaces [23,24]. Overall, the addition of EG has helped to reduce the friction and wear properties appreciably.

**3.3.1.3. Influence of temperature.** Based on the results from the above two parameters, it was observed that 7 phr filler loading is the optimum filler loading for improved wear resistance. Therefore, QMEG7 composites is subjected to wear tests by varying the temperatures and the results are illustrated in Table 5

It is interesting to note that COF and specific wear rate are the lowest at 30 °C and the highest at 50 °C. Intermediate values are observed at 100 °C [Fig. 9]. This change in COF and specific wear rate might be due to the change in wear mechanism. The main wear mechanism operating though the system is adhesive wear which might be changed at 50 °C as there is a sudden rise in temperature. The changes occurring through a

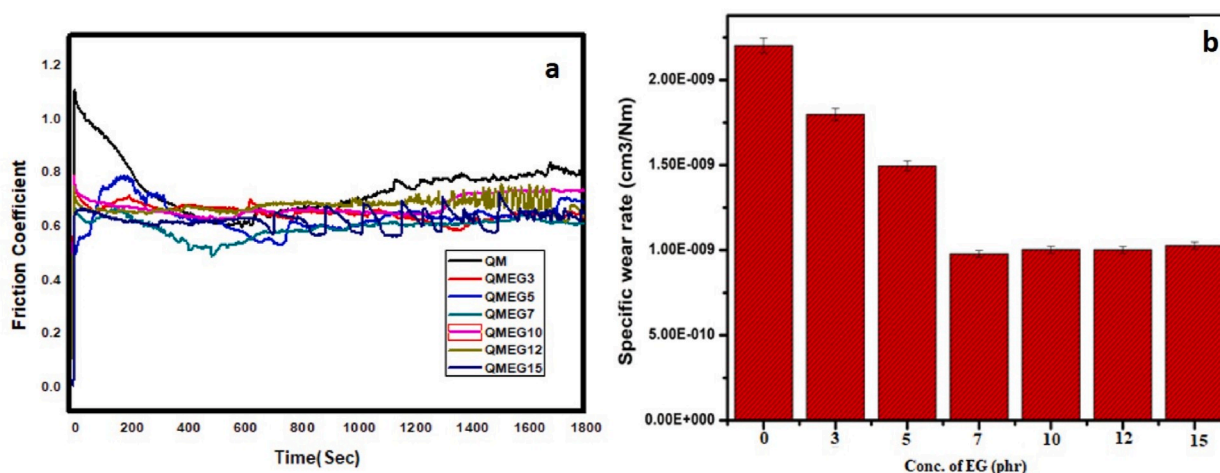


Fig. 7. (a) Friction coefficient of composites as a function of time (b) specific wear rate of the composites with various contents of EG (load-30 N, speed-2 m/s).

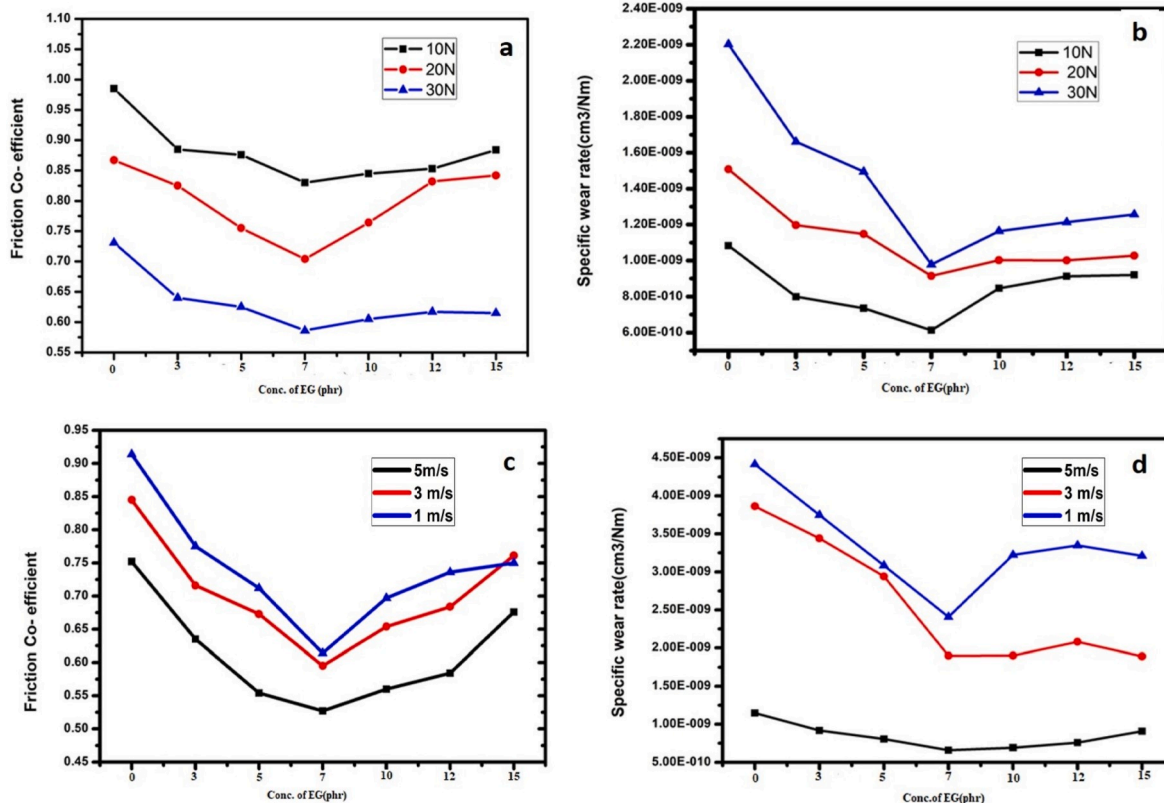


Fig. 8. (a) Friction coefficient (b) specific wear rate of composites with different loads (1800 m, RT, 2 m/s) and (c) Friction coefficient (d) specific wear rate of the composites with different sliding velocity (30 N, RT, 1800 mm).

Table 5  
COF and Specific Wear rate of QMEG7 composites with varying temperatures.

Temperature(°C)	Co efficient of friction	Specific wear rate × 10 <sup>6</sup> (mm <sup>3</sup> /Nm)
30	0.652	0.863
50	0.780	1.135
100	0.660	1.060

series of actions such as shear failure of adhesive points, de-bonding of EG particles, lubricant film formation, destruction and reformation etc. Further rise in temperature rearrange the system so that mechanism is more or less similar to an adhesive wear. The difference in temperature leads to activation energy changes and which causes change in the wear behaviour of the material. Moreover, this suggests that the composite has undergone physical and mechanical changes which could be due to the viscoelastic nature of the elastomeric composites [25].

### 3.3.2. Worn surface morphology

In order to understand the wear behavior of the prepared composites, SEM examinations of the specimens after the pin on disc tests were employed. Worn surface morphology of the developed composites with different filler reinforcement after being subjected to two body wear tests is shown in Fig. 9. During the wear tests, deformation of rubber specimens occurs leading to energy losses which mainly arises due to the hysteresis friction. Further, formation and destruction of adhesive points between the rubbing surfaces develops adhesive friction. As such, bulk hysteresis and contact adhesiveness comes into picture regarding the friction in rubber [26,27]. Fig. 10 shows the worn surface morphologies of the silicone composites embedded with different amounts of EG after sliding in a circular path of 50 mm in radius for about 30 min at a sliding velocity of 2 m/s under a normal load of 30 N. Small craters and ridge like patterns are visible on the surface of QM along the sliding direction because pure rubber has low mechanical properties. Because of this it could be easily torn and ruptured. These patterns lead to an increase in adhesion friction force which further increases the friction and wear properties. Also, without any reinforcing fillers wear rate is quite high in pure rubber. But as the EG content increases the surface becomes more flattened out. SEM image of QMEG5 reveals that localized material removal starts to take place. EG layers starts to chip off and sufficient stable lubricating films could be formed due to the extensive chipping of

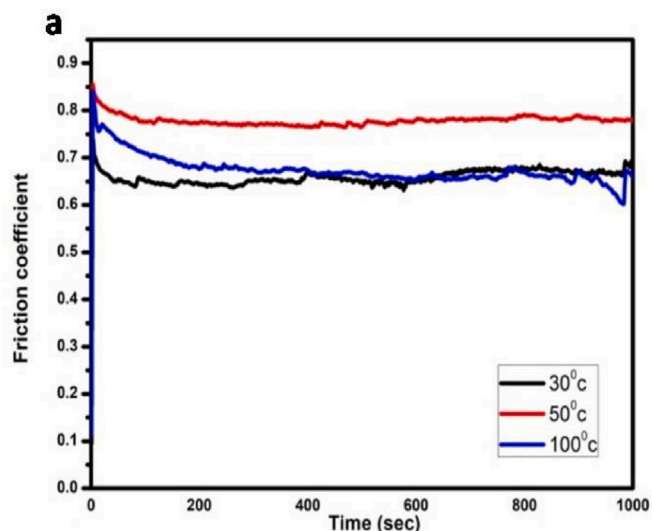


Fig. 9. Friction coefficient of QMEG7 composites as a function of temperature (30 N, 2 m/s, 1800 m).

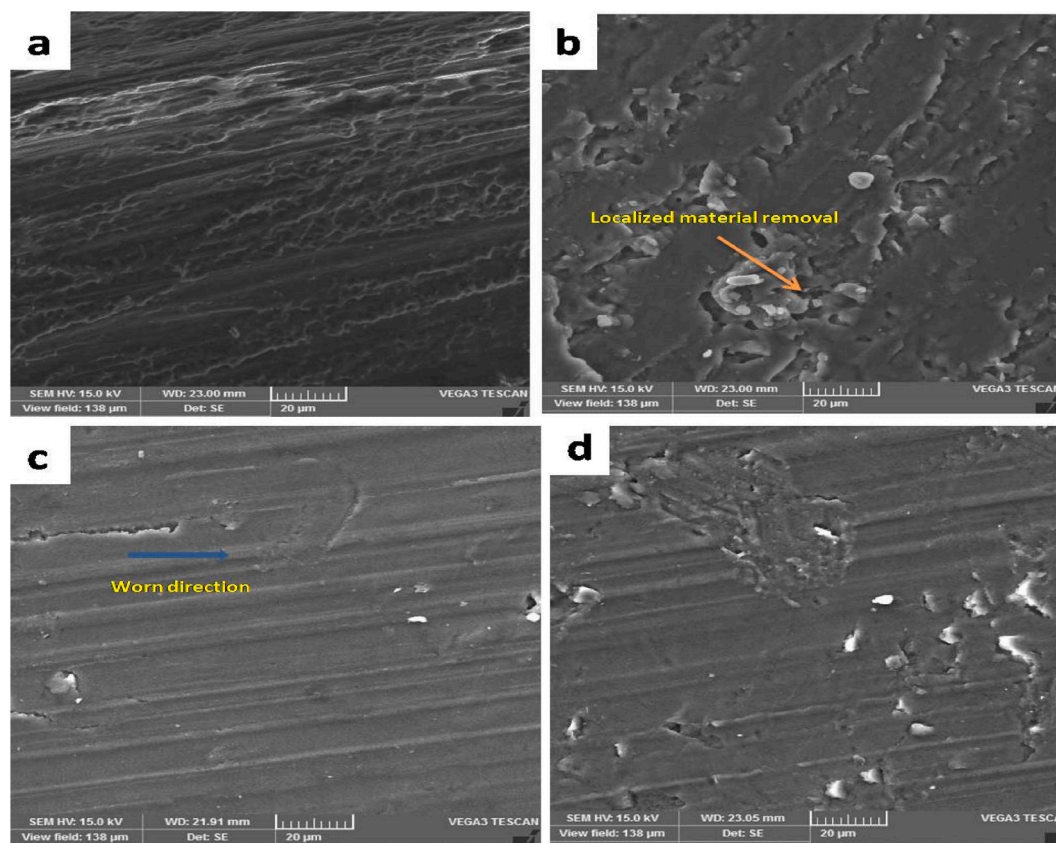


Fig. 10. SEM micrographs showing worn surface morphologies (a)QM(b)QMEG5(c)QMEG7 (d)QMEG10.

EG particles arising from slight abrasion of wear debris occurring between the rubbing surfaces. This leads to a decrease in adhesive friction.

However, almost a very neat surface morphology is present for the QMEG7 composite. Effective and stable lubricant film formation with the generation of sufficient chipped off EG particles have helped to reduce the friction and wear properties. This continuous stable film formation has reduced the real contact area of the rubbing surface which prevented further wear of the composite. Moreover, improved mechanical properties have been obtained for this composite when compared to neat rubber composite. This implies good dispersion of EG in the rubber matrix. Well dispersed filler within the rubber matrix leads to continuous and stable lubricant film formation. Since EG fillers have been easily chipped off, it indicates that poor interfacial adhesion exists and reducing the adhesive friction component. Further, with lesser number of interfacial adhesive points being created, results in reduced energy dissipations to shear the formed adhesive junctions. This results reduction in friction.

Addition of EG beyond the optimum value (7 phr) has affected this film formation. For composite with 10 phr EG surface morphology indicates material removal and shallow large crater during SEM examination. Beyond the optimum value, agglomeration has taken place and this has led to poor dispersion of EG within the composites. EG agglomerates have led to formation of strong interfacial adhesive junctions at the areas of agglomeration thus increasing the adhesive friction and hysteresis friction. From the SEM study it is concluded that wear of composites has occurred mainly due to adhesive wear. Initiation of adhesive wear starts with formation of interfacial adhesive junctions. When rubber starts to slide on rigid surface, with the applied load, deformation of rubber surface in contact takes place. The surface initially adheres together under dry sliding conditions. The relative sliding motion acts to shear the formed adhesive junctions and wear of the rubber material starts to occur. Therefore, wear mechanism involves

the formation of adhesive junctions, shear failure of adhesive points, debonding of EG particles, lubricant film formation, destruction and reformation, and finally, adhesive wear [28].

Silicone rubber exfoliated graphite composites were prepared and evaluated by (High Resolution Transmission Electron Microscopy) HR-TEM, as shown in Fig. 11. HR-TEM image of QMEG7 indicates that fine dispersion of exfoliated graphite with layered structure in the QM matrix. The graphene layers of the EG clearly seen from the figure without any agglomeration. The better dispersion of EG in QM matrix due to good interfacial interaction between EG and QM. EG act as reinforcing agent in QM matrix. It helps to transfer stress uniformly throughout the matrix and protect from external shocks.

The AFM (Atomic Force Microscopy) analysis was used to study the surface roughness values of the QMEG composites. Fig. 12 illustrates the surface topographical features of QM, QMEG5, QMEG7 and QMEG10 composites in 2D and 3D view. In QMEG7 sample the distribution and dimensions of the heaps or hills are almost homogeneous, which indicates a good dispersion of EG in the QM matrix. Addition of EG to the QM matrix increases the surface roughness Ra value. The improvement in mechanical and tribological properties compared to the gum samples can be correlated with AFM analyses. During tribological analyses, the homogeneous distribution of heaps and hills in QMEG7 sample helps to interact the counter surface uniformly. The SEM micrograph obtained from the QMEG7 vulcanisates showed a smooth surface. During tribological testing, the deformation rate QMEG7 was much lower than that of other composites. This distribution also helps to QMEG7 to form uniform transfer film in between material and counter surface, which improve the wear resistance of the material. In QMEG10, the surface roughness value was much higher around 77 nm which attributed to increased concentration of EG in QM matrix.

In roughness analysis, If Rms and Ra are similar, there is no layer deviation from the mean surface. The systems with Rms-Ra obtained a

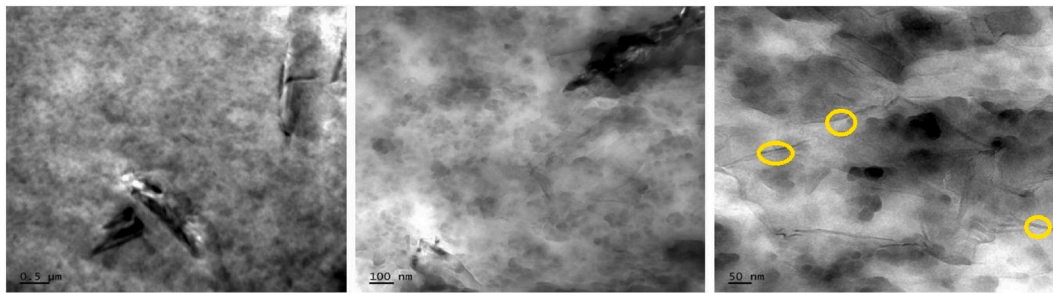


Fig. 11. TEM images of QMEG7 composite and yellow circle indicate the layers of EG. (For interpretation of the references to colour in this figure legend, the reader is referred to the Web version of this article.)

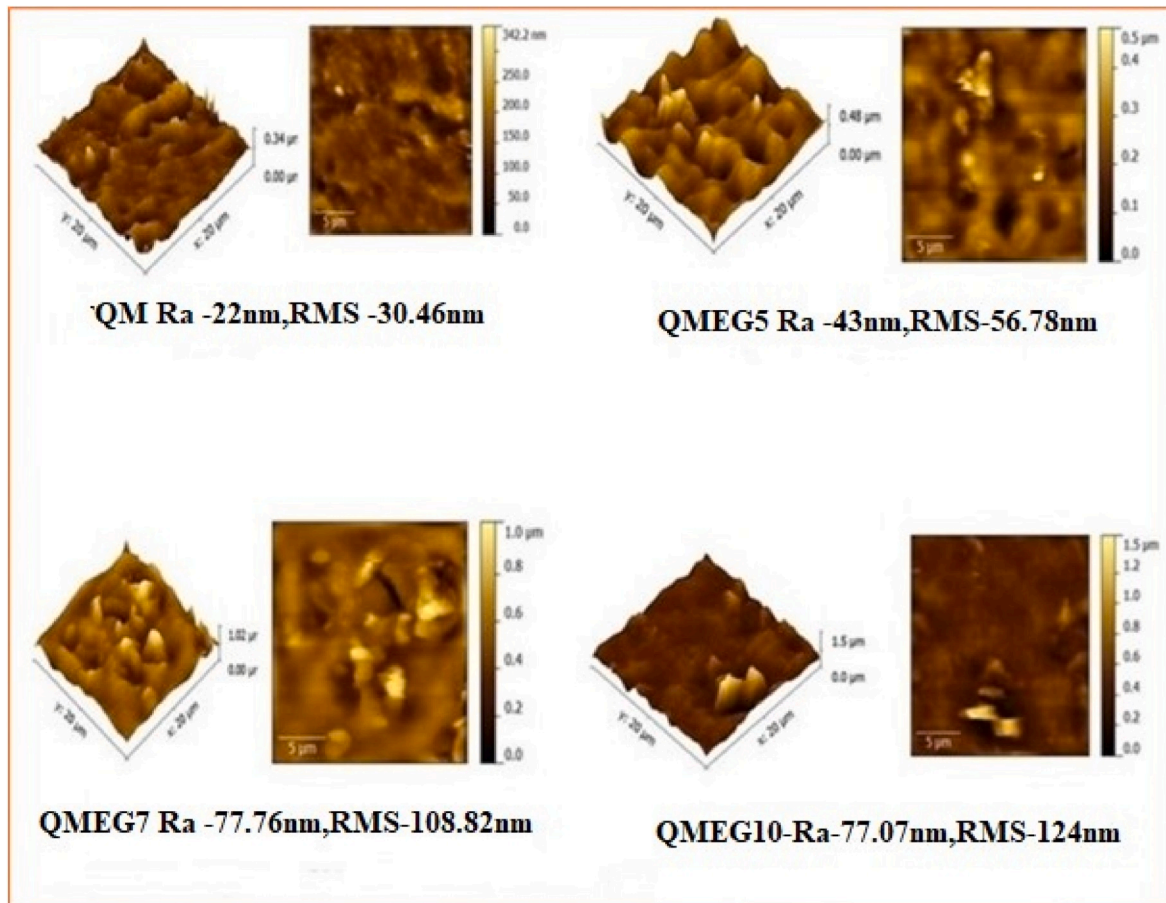


Fig. 12. AFM topography 2D and 3D images of silicon rubber exfoliated graphite composites with different EG content. (For interpretation of the references to colour in this figure legend, the reader is referred to the Web version of this article.)

higher value, it confirms the presence of filler particles on the surface [29]. From Table 6, it is clear that Rms-Ra value increased with filler loading. It confirms that EG comes on the surface of the composite and it interact with counter surface and produce thin film of lubricating film, which improve the material from wear resistance of the material.

**Table 6**  
Roughness analysis of QMEG composites.

Sample	Ra (nm)	Rms (nm)	Rms-Ra(nm)
QM	22.7	30.46	7.76
QMEG5	42.99	56.78	13.79
QMEG7	77.76	108.82	31.06
QMEG10	77.07	124	46.93

### 3.3.3. Wear properties [Three body wear tests]

Wear volume and specific wear rates of QMEG7 composites with different loads are shown in Table 7. The data reveals that wear volume and specific wear rate have increased as the load increases with a more dramatic increase for the latter.

Here, wear increases with an increase in load. The rubber might have

**Table 7**  
Wear volume and Specific wear rate of QMEG7 composite with different loads.

Load(N)	Wear volume(cm <sup>3</sup> )	Specific wear rate × 10 <sup>4</sup> (cm <sup>3</sup> /Nm)
2.94	1.1091	5.16
4.90	1.1686	9.25
9.80	1.2637	32.24

been induced with more stress with an increased load. This might have been substantial in weakening the interfacial interaction between the silicone rubber and the EG particles. As such, more EG particles and rubber were subjected to abrasive action further increasing the material removal rate. Moreover, as the load is increased more EG particles flake off and the high loads prevents the formation of stable lubricating film between the abrading surfaces by this flaked off EG particles.

### 3.4. Dielectric properties

The variations in electrical properties of the developed composites with the addition of fillers has been analysed. Fig. 13 (a) depicts the variation of AC conductivity as function of frequency and filler loading. The AC Conductivity (S/cm) of the developed composites is not only found to increase with an increase in frequency but also with filler loading. Composites with 15phr filler loading achieved higher values of conductivity. With more filler particles inside the filler material, the distance between the particles decreases and charges will be able to hop or tunnel [30] depending on the applied frequency. The increase in value with increased filler loading is due to better dispersion of EG which leads to micro capacitor network formations within the composites.

The material's ability to store an electric field in the polarisation of the medium is given by the measure of its dielectric permittivity and Fig. 13 (b) shows dielectric permittivity versus frequency and filler loading graph. It could be seen that for the neat QM sample, a slight

decrease in the dielectric permittivity ( $E'$ ) occurs with increasing frequency. A similar pattern can also be observed for QMEG3, QMEG5, QMEG7 and QMEG10 sample although the value of  $E'$  increased slightly when compared to that of neat sample.

The elastomeric composites attained the percolation threshold ( $p_c$ ) at filler loading of 12 phr and showed a sudden increase in dielectric constant at low frequencies. This implies that there were many EG particles separated by thin layers of QM. As the filler loading increases the permittivity increases at lower frequencies. The permittivity value increased with increasing the content of EG suggests the increased energy storage capacity of the developed composites [31–33]. However, it decreases with an increase in frequency. The number and the ability of the orientable dipoles to orient under applied electric field determines the dielectric permittivity value of the composites. At lower frequency, dipoles are able to orient under applied field and results in better filler-filler networks within the composites. Moreover, Maxwell–Wagner–Sillars relaxation [34] also occurs at low frequencies and therefore interfacial polarisation leads to an increase in permittivity initially. The polymer chains are unable to orient at higher frequencies and thus a decrease in value of the permittivity is observed. Fig. 13 (c) gives the variation of dielectric loss with frequency and filler loading. Dielectric loss represents extent of energy dissipation due to charge migration or conversion to thermal energy in the case of dielectric loss of QM composites. Energy dissipation is observed to be very low for all composites except QMEG15. Hence, QM composites with increased AC conductivity decreased dielectric loss and increased dielectric

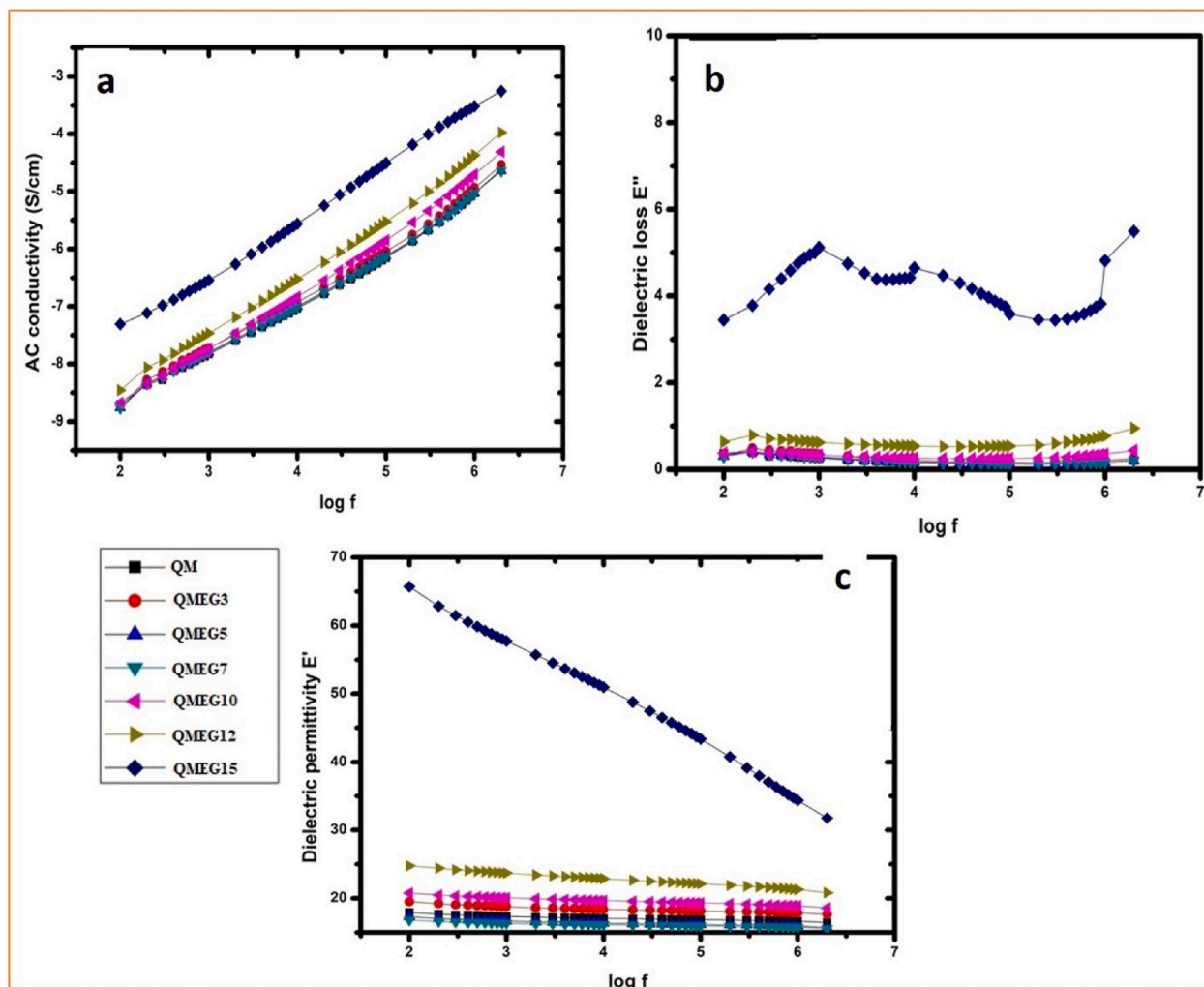


Fig. 13. Effect of EG loading and frequency on (a) AC Conductivity (b) Dielectric permittivity and (c) Dielectric loss of the composites.

permittivity has been developed. The resulting increase in dielectric properties is because of better adhesion between filler material and QM matrix [35,36].

#### 4. Conclusion

Novel Silicone Rubber composites with Exfoliated Graphite as reinforcing fillers were successfully developed first time using simple two roll mixing technique. On investigating the composite properties, the experimental data reveals its excellent mechanical, tribological and dielectric properties and therefore it could be applied in automobile and aerospace applications.

- Silicone rubber with 7 phr of exfoliated graphite composite exhibited the highest mechanical properties as it evident from the fracture surface morphology of the composite. Coefficient of friction and specific wear rate reduced as the exfoliated graphite content increased. As the increased load reduces coefficient of friction but increases specific wear rate, while the increased sliding velocity increases both coefficient of friction and specific wear rate. COF and specific wear rate values were increased with increase in temperature upto 50 °C and then decrease. This might be due to the change in adhesive wear mechanism operating though the system at 50 °C as there is a sudden rise in temperature.
- Silicone rubber with 7 phr of exfoliated graphite composite has the lowest coefficient of friction value and silicone rubber with 10phr of exfoliated graphite composite sample quickly stabilized its friction value.
- Among the various composites, silicone rubber with 7 phr of exfoliated graphite composite recorded decreased friction and wear properties. A very neat worn surface morphology was also obtained for Silicone rubber with 7 phr of exfoliated graphite composite. Wear in the composite mainly occurred due to adhesive wear between the surfaces in contact.
- Under three body tests of silicone rubber with 7 phr of exfoliated graphite composite, wear volume and wear rate were found to increase as the load increases.
- AFM and TEM analysis confirms the better dispersion of EG particles, presence of EG particle on the composite surface form a lubricant film and improved wear resistance.
- Increased AC conductivity and dielectric permittivity, decreased dielectric loss were obtained with silicone rubber with 15phr of exfoliated graphite composites showing enhanced dielectric performance.

Therefore, incorporating EG as a reinforcing filler is found to be excellent in preparing filler reinforced elastomeric composites.

#### Declaration of competing interest

Authors have no conflict of interest.

#### CRediT authorship contribution statement

**P.S. Sarath:** Conceptualization, Data curation, Formal analysis, Investigation, Writing - original draft. **Sohil Varghese Samson:** Data curation, Formal analysis, Writing - original draft. **Rakesh Reghunath:** Conceptualization, Writing - original draft, Formal analysis, Visualization, Investigation. **Mrituanjay Kumar Pandey:** Visualization, Validation. **Józef T. Haponiuk:** Writing - review & editing, Supervision. **Sabu Thomas:** Conceptualization, Supervision, Writing - review & editing. **Soney C. George:** Conceptualization, Project administration, Resources, Supervision, Writing - review & editing.

#### Acknowledgment

The authors are especially grateful to DRDO (Order No: ERIP/ER/1504758/M/01/1667), New Delhi, India for providing the financial assistance. International and Inter University Centre for Nanoscience and Nanotechnology, Mahatma Gandhi University, Kottayam, Kerala, India and Rubber Park Airapuram, Kerala, India are also acknowledged here for various analyses.

#### Appendix A. Supplementary data

Supplementary data to this article can be found online at <https://doi.org/10.1016/j.polymeresting.2020.106601>.

#### Nomenclature

AFM	Atomic Force Microscopy
COF	Friction coefficient
DCP	Dicumyl peroxide
1D	One Dimensional
2D	Two dimensional
3D	Three Dimensional
EG	Exfoliated Graphite
HNT	Halloysite nanotube
M <sub>H</sub>	Maximum Torque
M <sub>L</sub>	Minimum Torque
QM	Silicone Rubber
QMEG	Exfoliated graphite/silicone rubber composite
Ra	Arithmetic average of the absolute values of surface height deviation taken from the mean plane
Rms	Root mean square average of surface height deviation taken from the mean data
SEM	Scanning electron Microscopy
TEM	Transmission electron microscopy
XRD	X-ray diffraction
UHMWPE	Ultrahigh Molecular Weight Polyethylene

#### References

- [1] T. Jose, G. Moni, S. Salini, A.J. Raju, J.J. George, S.C. George, Multifunctional multi-walled carbon nanotube reinforced natural rubber nanocomposites, *Ind. Crop. Prod.* 105 (2017) 63–73, no. April.
- [2] J. Abraham, M. Arif P, P. Xavier, S. Bose, S.C. George, N. Kalarikkal, S. Thomas, Investigation into Dielectric Behaviour and Electromagnetic Interference Shielding Effectiveness of Conducting Styrene Butadiene Rubber Composites Containing Ionic Liquid Modified MWCNT, *Polym. (United Kingdom)* 112 (2017) 102–115.
- [3] M.G. Maya, S.C. George, T. Jose, L. Kailas, S. Thomas, Development of a flexible and conductive elastomeric composite based on chloroprene rubber, *Polym. Test.* 65 (2018) 256–263, no. September 2017.
- [4] G. Moni, A. Mayeen, J. Abraham, T. Jose, M.G. Maya, R. Bhowmik, S.C. George, Flexible FKM/mRGO nanocomposites with excellent thermal, mechanical and electrical properties, *Arab. J. Chem.* 13 (1) (January 2020) 2142–2152.
- [5] K.K. Sadasivuni, D. Ponnamma, S. Thomas, Y. Grohens, Evolution from graphite to graphene elastomer composites, *Prog. Polym. Sci.* 39 (4) (Apr. 2014) 749–780.
- [6] SinEtsu, Characteristic properties of Silicone Rubber Compounds Meeting the increasingly diverse and sophisticated needs of industry with the unique properties of silicone rubbers, 2013.
- [7] J.-H. Lee, W.Y. Ji, Electrical and mechanical properties of silicone rubber for high voltage insulation, *Prop. Appl. Dielectr. Mater.* 2003. Proc. 7th Int. Conf. 2 (2003) 591–594, vol. 2.
- [8] L. Jiang, A. Betts, D. Kennedy, S. Jerrams, Improving the electromechanical performance of dielectric elastomers using silicone rubber and dopamine coated barium titanate, *Mater. Des.* 85 (2015) 733–742.
- [9] W. Du, Z. Zhang, W. Fan, W. Gao, H. Su, Z. Li, Fabrication and evaluation of polydimethylsiloxane modified gelatin/silicone rubber asymmetric bilayer membrane with porous structure, *Mater. Des.* 158 (2018) 28–38.
- [10] R. Berahman, M. Raiati, M. Mehrabi Mazidi, S.M.R. Paran, Preparation and characterization of vulcanized silicone rubber/halloysite nanotube nanocomposites:effect of matrix hardness and HNT content, *Mater. Des.* 104 (2016) 333–345.
- [11] C. Xu, Y. Wang, B. Lin, X. Liang, Y. Chen, Thermoplastic vulcanizate based on poly(vinylidene fluoride) and methyl vinyl silicone rubber by using fluorosilicone rubber as interfacial compatibilizer, *Mater. Des.* 88 (2015) 170–176.

- [12] J. Bai, X. Liao, E. Huang, Y. Luo, Q. Yang, G. Li, Control of the cell structure of microcellular silicone rubber/nanographite foam for enhanced mechanical performance, *Mater. Des.* 133 (2017) 288–298.
- [13] Y. Song, J. Yu, L. Yu, F.E. Alam, W. Dai, C. Li, N. Jiang, Enhancing the thermal, electrical, and mechanical properties of silicone rubber by addition of graphene nanoplatelets, *Mater. Des.* 88 (2015) 950–957.
- [14] L. Gan, S. Shang, C.W.M. Yuen, S.X. Jiang, N.M. Luo, Facile preparation of graphene nanoribbon filled silicone rubber nanocomposite with improved thermal and mechanical properties, *Compos. B Eng.* 69 (2015) 237–242.
- [15] P. Huang, Z. Xia, S. Cui, 3D printing of carbon fiber-filled conductive silicone rubber, *Mater. Des.* 142 (2018) 11–21.
- [16] T. Pyllos and D. E. T. Shepherd, “Wear of medical grade silicone rubber against titanium and ultrahigh molecular weight polyethylene,” *J. Biomed. Mater. Res. B Appl. Biomater.*, vol. 84B, no. 2, pp. 520–523.
- [17] Q. He, A. Li, Y. Zhang, S. Liu, Y. Guo, L. Kong, A study on mechanical and tribological properties of silicone rubber reinforced with white carbon black, *Tribol. Mater. Surface Interfac.* 12 (1) (2018) 9–16.
- [18] J. Frohlich, W. Niedermeier, H.-D. Luginsland, The effect of filler–filler and filler–elastomer interaction on rubber reinforcement Composites: Part A 36 (2005) 449–460.
- [19] S.C. George, K.N. Ninan, G. Groeninckx, S. Thomas, Styrene–butadiene rubber/natural rubber blends: morphology, transport behavior, and dynamic mechanical and mechanical properties, *J. Appl. Polym. Sci.* 78 (6) (2000) 1280–1303.
- [20] G. Moni, T. Jose, S. Rajeevan, A. Mayeen, A. Rejimon, P.S. Sarath, S.C. George, Influence of exfoliated graphite inclusion on the thermal, mechanical, dielectric and solvent transport characteristics of fluoroelastomer nanocomposites, *J. Polym. Res.* 27 (3) (2020) 1–11.
- [21] G. Kraus, Swelling of filler-reinforced vulcanizates, *J. Appl. Polym. Sci.* 7 (3) (1963) 861–871.
- [22] L. Liu, F. Yan, F. Gai, L. Xiao, L. Shang, M. Li, Y. Ao, Enhanced tribological performance of PEEK/SCF/PTFE hybrid composites by graphene, *RSC Adv.* 7 (53) (2017) 33450–33458.
- [23] L.L. Wang, L.Q. Zhang, M. Tian, Mechanical and tribological properties of acrylonitrile-butadiene rubber filled with graphite and carbon black, *Mater. Des.* 39 (2012) 450–457.
- [24] L. Wang, L. Zhang, M. Tian, Effect of expanded graphite (EG) dispersion on the mechanical and tribological properties of nitrile rubber/EG composites, *Wear* 276–277 (2012) 85–93.
- [25] A. Saffar, A. Shojaei, M. Arjmand, Theoretical and experimental analysis of the thermal, fade and wear characteristics of rubber-based composite friction materials, *Wear* 269 (1–2) (2010) 145–151.
- [26] Hysteresis losses in the friction of lubricated rubber: david tabor. *Rubber chemistry and technology*. V. 33. No. 1, jan.–mar. 1960, p. 142–150. (Reprinted from the Proceedings of the first international skid prevention conference, Virginia council of high, *Wear* 3 (5) (1960) 405.
- [27] J.A. Greenwood, D. Tabor, The friction of hard sliders on lubricated rubber: the importance of deformation losses, *Proc. Phys. Soc.* 71 (6) (1958) 989.
- [28] 12 Adhesion and Adhesive Wear, in: G.W. Stachowiak, A.W. Batchelor (Eds.), *Engineering Tribology*, 24, Elsevier, 1993, pp. 613–635.
- [29] C. Soney, George Regitha Rajan, Aprem Santhosh, The fabrication and properties of natural rubber-clay nanocomposites, *Polym. Test.* 51 (2016) 165–173. May.
- [30] J.P. Giltrow, A relationship between abrasive wear and the cohesive energy of materials, *Wear* 15 (1) (1970) 71–78.
- [31] M. Vaziri, R.T. Spurr, F.H. Stott, An investigation of the wear of polymeric materials, *Wear* 122 (3) (1988) 329–342.
- [32] S. Capaccioli, M. Lucchesi, P.A. Rolla, G. Ruggeri, Dielectric response analysis of a conducting polymer dominated by the hopping charge transport Dielectric response analysis of a conducting polymer dominated by the hopping charge transport, *J. Phys. Condens. Matter* 10 (1998) 5595–5617.
- [33] J. Abraham, L. Kailas, N. Kalarikkal, S.C. George, S. Thomas, Developing highly conducting and mechanically durable styrene butadiene rubber composites with tailored microstructural properties by a green approach using ionic liquid modified MWCNTs, *RSC Adv.* 6 (39) (2016) 32493–32504.
- [34] S. Agrawal, K.S. Ojha, D. Sahu, Structural and dielectric studies of MWCNT reinforced microcellular silicone elastomer nanocomposite, *Mater. Today Proc.* 2 (9) (2015) 4516–4520.
- [35] E. Tuncer, S.M. Gubanski, Electrical properties of filled silicone rubber, *J. Phys. Condens. Matter* 12 (8) (2000) 1873.
- [36] M. Samet, V. Levchenko, G. Boiteux, G. Seytre, A. Kallel, A. Serghei, Electrode polarization vs. Maxwell-Wagner-Sillars interfacial polarization in dielectric spectra of materials: characteristic frequencies and scaling laws, *J. Chem. Phys.* 142 (19) (2015).